

## Article

# Fire Protection of Steel Structures of Oil and Gas Facilities: Multilayer, Removable, Non-Combustible Covers

Marina Gravit <sup>1</sup>, Vasiliy Prusakov <sup>2</sup>, Nikita Shcheglov <sup>1</sup> and Irina Kotlyarskaya <sup>1,\*</sup>

<sup>1</sup> Peter the Great St. Petersburg Polytechnic University, 195251 St. Petersburg, Russia; marina.gravit@mail.ru (M.G.); tsheglov.ne@edu.spbstu.ru (N.S.)

<sup>2</sup> LLC "RPC PROMIZOL", 121087 Moscow, Russia; v.prusakov@tdpromizol.com

\* Correspondence: vasilieva\_il@spbstu.ru

**Abstract:** Fire protection is required to protect metal structures of oil and gas facilities from fires. Such fire protection should provide high fire resistance limits: 60, 90, 120 and more minutes. Specialists of LLC "RPC PROMIZOL" developed a multilayer, removable type of fire protection made of superfine basalt fibre and ceramic materials for operation in Arctic conditions. Five experimental studies were carried out in standard and hydrocarbon fire regimes. The fire protection effectiveness of the products for I20 beams without load was obtained: a 50 mm thick coating provided 130 min of a standard fire regime; a 15 mm thick coating provided 60 min. The 15 mm thick coating provided 30 min of a hydrocarbon fire regime and the 50 mm thick coating provided 93 min of a hydrocarbon fire regime. The I40 beam under a load of 19.9 tf showed an R243 for the standard fire regime. The coefficients of effective thermal conductivity and specific heat capacity of fire-retardant compositions were determined by solving the inverse heat conduction problem. The problem was solved by modelling using the QuickField 7.0 software package, which implements FEM. Modelling showed that for obtaining the fire resistance limit R120 under the standard fire regime for the sample steel structure from an I40 beam, it is enough to apply fire protection with a thickness of 25 mm instead of 50 mm, which agrees with the experimental data. For the hydrocarbon regime, it is predicted that R120 can be obtained at a thickness of 45 mm instead of 50 mm.

**Keywords:** buildings; oil and gas facility; fire resistance; fire protection; structural protection; removable fireproofing; Arctic climate; fireproof fabric; basalt fibre



**Citation:** Gravit, M.; Prusakov, V.; Shcheglov, N.; Kotlyarskaya, I. Fire Protection of Steel Structures of Oil and Gas Facilities: Multilayer, Removable, Non-Combustible Covers. *Fire* **2024**, *7*, 86. <https://doi.org/10.3390/fire7030086>

Academic Editors: Fang Liu, Shengzhong Zhao and Longxing Yu

Received: 31 January 2024

Revised: 5 March 2024

Accepted: 9 March 2024

Published: 14 March 2024



**Copyright:** © 2024 by the authors. Licensee MDPI, Basel, Switzerland. This article is an open access article distributed under the terms and conditions of the Creative Commons Attribution (CC BY) license (<https://creativecommons.org/licenses/by/4.0/>).

## 1. Introduction

Buildings and structures located at the poles are Arctic stations and plants for oil and gas production, processing and transportation. Steel bearing and enclosing structures of such facilities should be protected with special materials; in particular, fire protection means increasing their fire resistance limits [1–3]. There are precedents for offshore platform fires, such as the world's largest offshore platform disaster, Piper Alpha, in the North Sea, which led to a series of explosions on major oil and gas pipelines [4–6]. The Deepwater Horizon platform fire and explosion resulted in loss of life, destruction and a negative environmental impact and is considered the largest industrial disaster [7,8]. Fires have also occurred at Arctic and Antarctic stations, whose supporting elements are steel structures. For example, a fire destroyed the Commander Ferraz Antarctic research station located on King George Island in Antarctica [9,10].

Various fire protection coating systems are used to protect the metal structures of floors and trestles of oil and gas facilities from low (in case of cryogenic liquids spilling) and high (in case of possible development of hydrocarbon fire regime) temperatures. Requirements for the fire resistance limits of structures are fixed in the normative documents of oil and gas complexes, for example, in international standards, American and Norwegian standards, and standards of large concerns based on fire risk calculations [11].

There are three main methods of fire protection for steel structures: intumescent coatings [12–15], plaster compositions [16] and structural fire protection [17–19]. Figure 1 shows a scheme of the means and methods of fire protection for steel structures used at oil and gas facilities [20].

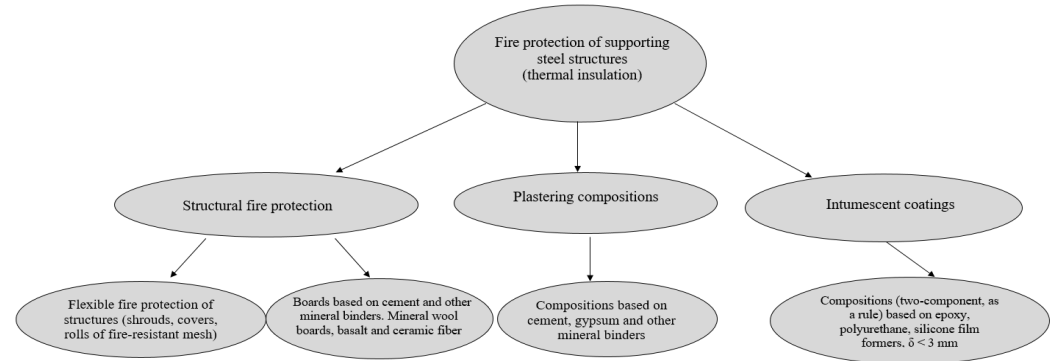


**Figure 1.** Means and methods of fire protection for steel structures for the oil and gas industry.

According to the Code of Practice [21], the Arctic climate belongs to category 3, “most severe conditions”, with absolute minimum temperatures between  $-54\text{ }^{\circ}\text{C}$  and  $-71\text{ }^{\circ}\text{C}$ . According to the Köppen international climate classification, the Arctic belongs to polar zone E [22]. Zone E is a group of zones, namely, “Et – tundra” and “Ef – ice cap zone”, which are characterized by permanent snow cover and average temperatures below  $10\text{ }^{\circ}\text{C}$ .

In polar conditions, the following requirements are imposed for the fire protection of building structures: preservation of reliability (serviceability) in the Arctic climate for at least 10 years, ease of installation and replacement, and resistance to extreme effects in the form of liquid hydrocarbon spills, with the subsequent ignition and development of a hydrocarbon fire regime [23–26]. Fire protection in the form of intumescent coatings and plasters is of little use in such conditions since these are wet processes.

Such requirements are best satisfied by structural fire protection, which is often used in harsh climatic conditions. Thus, in [27], experiments on an example of steel structures with structural fire protection based on basalt superfine fibres in the Arctic region were conducted to evaluate various means of fire protection, the results of which showed that the most effective coatings for harsh Arctic conditions are materials containing basalt superfine fibres. Structural protection based on boards with various binders has a number of significant advantages over other types: it provides high fire resistance limits from 120 min and higher for structures, even with a small cross-section; relative ease of installation; and resistance to climatic conditions. The disadvantages of board materials include the possibility of cracking when the structure is loaded. For example, [28] shows that using gypsum slabs up to 20 mm thick to protect reinforced concrete columns exposed directly to fire flames reduces by one-third the amount of heat penetration during the period of higher exposure compared to unprotected ones. However, the slabs show significant displacement.

The most common thermal insulation materials in applied means of fire protection for structures are thermal insulation wools of various types, and about 60% of all used thermal insulation uses fibre materials: glass, mineral and basalt wool based on fine and ultrafine fibres [29]. In [30], a roll crosslinking material made of ultrafine basalt fibre with a thickness from 5.0 to 16.0 mm, laminated on one side with aluminium foil, was considered. The fire resistance limit of the fireproofing material was EI90.

The results of [31] confirm that basalt fibre has the greatest advantages for the production of flame-retardant fabric. Thus, basalt fibre is widely used in fire retardant materials, shrouds, curtains and covers both on structures and on products to ensure high fire resistance limits [32–34].

To predict the fire resistance limits of structures, including those with fire protection, calculations in modern software packages using the finite element method are used. In [35], a FEM model (ANSYS 15 software) was used for double-slope brick cladding depending on

the position of a steel-framed column with different types of fire protection. The modelling showed that fire protection in the form of a 30 mm thick layer of rock wool allowed a temperature of 500 °C to be reached in 7.5 min on an unheated surface; a 40 mm thick layer reached this temperature in 8.5 min and a 50 mm thick layer reached it after more than 60 min.

In [36,37], the authors conducted experimental and numerical studies (Abacus 2023 software was used) to study the characteristics of loaded glass fibre-reinforced polymer beams under standard fire conditions.

For the oil and gas industry, fire protection for metal structures requires non-combustible thermal insulation materials that do not contain flammable polymers and that do not crack under load. Such combined materials, stitched with non-combustible threads and fasteners, can be used to protect shut-off equipment and various valves and critical sections of pipelines, as well as for the manufacture of covers for valves [38–40]. However, such solutions are not used practically for the protection of building structures.

Specialists of LLC “RPC PROMIZOL” (Moscow, Russia) [41] developed a multi-layer, removable type of fire protection made of superfine basalt fibre and ceramic materials for Arctic LNG 2. [42], a project of NOVATEK Gas Concern (Moscow, Russia) on the Yamal Peninsula in the Arctic climate of Russia related to the production of liquefied natural gas. A programme of experimental research was developed, including a study of the effect of a fire regime on steel according to ASTM-119 [43] and its analogue for the temperature curve of the standard [44] and hydrocarbon fire regimes, according to UL 1709 [45] and its European analogue EN 1363-2 [46] in terms of the hydrocarbon fire regime.

This paper presents data on the study of combined coating for steel structures based on BSTFs and ceramic fibres during fire tests with standard and hydrocarbon temperature regimes with different layer thicknesses. By solving the inverse problem of heat conduction using a numerical model, the thermophysical characteristics of the flame retardant composition were obtained. The optimization problem of the reduction of material consumption at the achievement of necessary fire protection efficiency was solved.

## 2. Materials and Methods

### 2.1. Materials

Basalt superfine fibres (BSTFs) have an elementary fibre thickness of 1–3 µm and a length of more than 50 mm, while basalt fine fibres (BFTs) have an elementary fibre thickness of 5–15 µm and a length of up to 50 mm (Figure 2). Glass fibre, slag fibre and mineral fibre are also called fine fibre because the average diameter of these fibres is 4–12 µm. This structure of fine fibres deprives the product of strength. Therefore, phenol formaldehyde or other organic resins are used to bind thin fibres at an amount of 2–10% [29]. Reducing the fibre diameter leads to an increase in the thermal resistance of the material due to a decrease in the contact area between the fibres [29,47].



**Figure 2.** Basalt fibres: (a) basalt superfine fibres with fibre diameter 1–3 µm; (b) basalt ultrafine fibres with fibre diameter 0.6–1 µm; (c) basalt microfine fibres with fibre diameter less than 0.6 µm [48].

When changing the diameter from 0.6 to 20 µm, the thermal conductivity increases from 0.0237 to 0.375 at  $t = 25$  °C. Thus, the optimal density of laying in the thermal insulation structure should be 80–110 kg/m<sup>3</sup> for BSTF wool, 140 kg/m<sup>3</sup> for BSTF, 150–160 kg/m<sup>3</sup> for glass wool and about 200 kg/m<sup>3</sup> for slag wool. Thus, achieving the same thermal

conductivity characteristics of basalt superfine fibre products requires several times less density than that for basalt fine fibre, glass wool and slag wool products [29].

The multifunctional thermal insulation system PROIMZOL-MIX PROPLATE (manufacturer LLC “RPC PROMIZOL”, Moscow, Russia) is a fireproof composite coating consisting of a combination of non-combustible materials, glass fibre and silica, and is a flexible roll web that is fixed with special tapes and fasteners [49].

A multilayer product for the fire protection of building structures is an insulating cover made of non-combustible, flexible, multilayer materials. The layers of the cover are sewn together with non-combustible and heat-resistant ceramic, glass fibre or silica threads. The cover is stitched with clamp fire-resistant tapes, which are made of twisted basalt and silica yarns and have a self-tightening fastening knot for fixing the cover that is stretched on building structures. A scheme of the composite layers of this product is presented in Figure 3.

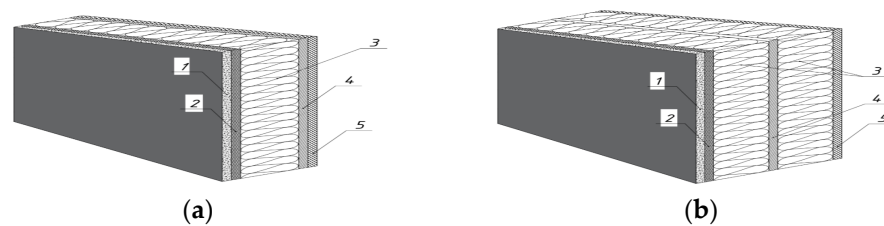


**Figure 3.** Composite layers of the product: (a) under conditions of standard (cellulose)-type combustion and (b) under conditions of hydrocarbon-type combustion, where 1—heat-strengthened basalt fabric, 2—ceramic fibre fabric, 3—mineral wool, 4—metal alloy sheets, 5—glass cloth [49].

A multifunctional thermal insulation system contains BSTFs and mineral wool with a density of at least  $100 \text{ kg/m}^3$ . BSTF is a layer of staple fibres with a diameter of 1 to 3 microns, intertwined and bound with ether in the form of high-quality basalt fibre canvas. The content of solid non-fibre inclusions larger than 0.25 mm does not exceed 10% of the total filler fraction. The cover is wrapped with silica cloth with a vermiculite filler. The tapes are made of twisted basalt and silica threads in the ratio of 70–90% basalt thread to 30–10% silica thread. Technical characteristics of the tape: width 10–50 mm; linear density not less than 002 kg/min; working temperature range from  $-200 \text{ }^\circ\text{C}$  to  $+1200 \text{ }^\circ\text{C}$ .

The tapes are sewn to the cover and are one piece with it (which is especially important for cases of complex shape, for example, fastening nodes or joints, where the tightening line must be precisely defined). The fastener design is robust and designed for repeated use.

The total density of the cover is  $125\text{--}130 \text{ kg/m}^3$  and depends on the product configuration. Temperature shrinkage is up to 3%.

## 2.2. Methods

### 2.2.1. Experimental Studies

The experiments were carried out for sample nos. 1–4 in accordance with [50]. For an I-beam with height  $(1700 \pm 10) \text{ mm}$  profile 20B1 [51] and a volume coefficient of  $294 \text{ m}^{-1}$  [52], the covers were wrapped and strapped (Figure 4). The temperature at which the metal of the samples on the unheated surface reached the critical temperature of  $500 \text{ }^\circ\text{C}$  was taken as the limit state.

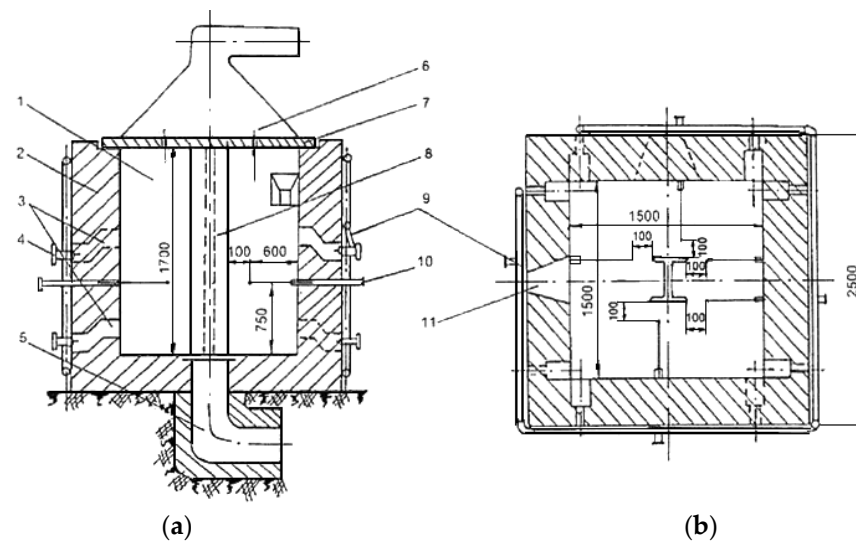


**Figure 4.** The furnace according to GOST 53295-2009 [50] for nos. 1–4: (a) main view and (b) top view, where (1) is a fire chamber, (2) is a furnace masonry, (3) is a nozzle heating channel, (4) is a nozzle, (5) is a smoke duct, (6) is an exhaust umbrella, (7) is a furnace vault, (8) is a test sample, (9) is an air duct, (10) is a thermocouple, (11) is an inspection hatch.

Specimen no. 5 was a column of I-beam profile no. 40IK with a height of  $(2700 \pm 10)$  mm and was tested under a static load of 195.22 kN (19.9 tf). The tests were carried out in accordance with [51,52] (Figure 5). The type of sample was selected by the customer. The specimen was equipped with 40 mm thick support plates under the condition of vertical compression, with articulated resting on one side and rigid pinching on the other side of the column. The vertical strain after loading was 0.7 mm.

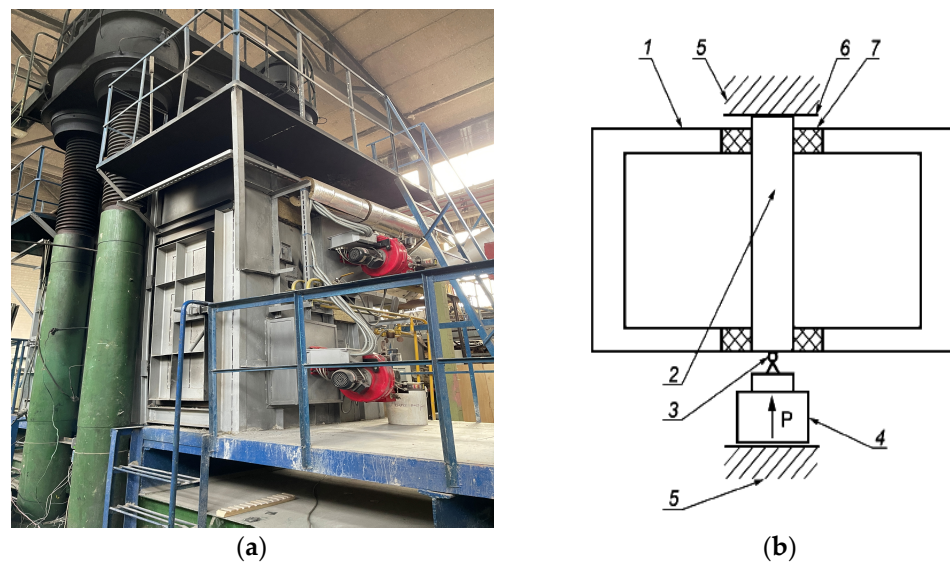


**Figure 5.** Test sample no. 5 in the furnace (a) before the test and (b) the schematic diagram of the installation for firing tests of a steel column under load [53], where (1) is the firing chamber of the furnace, (2) is a prototype of a steel column, (3) is a hinged support, (4) is a loading device, (5) is upper and lower support elements that ensure the operation of the loading system of the prototype, (6) is a device for hard clamping of the prototype, (7) is thermal insulation.

In Figure 6, the cross-sections of the I-beams for specimen nos. 1–4 and specimen no. 5 and the locations of thermocouple installation are shown (Figure 6a).

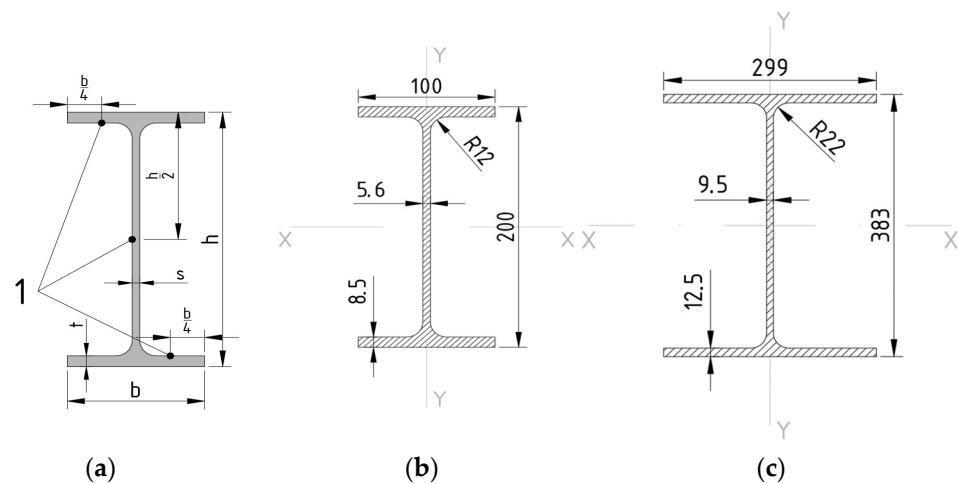


Figure 6. I-beam: (a) general view, (b) I-beam profile IB20, (c) I-beam profile IK40.

Table 1 shows the characteristics of the cross-sections of the I-beams.

Table 1. Cross-section characteristics of the IB20 and I40K beams.

| Type                    | h, mm | b, mm | S, mm | t, mm | R, mm | F, cm <sup>2</sup> | I <sub>x</sub> , cm <sup>4</sup> | I <sub>y</sub> , cm <sup>4</sup> |
|-------------------------|-------|-------|-------|-------|-------|--------------------|----------------------------------|----------------------------------|
| 20B1, sample nos. 1–4   | 200   | 100   | 5.6   | 8.5   | 12    | 28.49              | 1943                             | 142.3                            |
| IK40-beam, sample no. 5 | 383   | 299   | 9.5   | 12.5  | 22    | 112.91             | 30,556                           | 5575.4                           |

Tests of sample nos. 2 and 4 were carried out until a temperature of 500 °C was reached during the firing process under the condition of creating a hydrocarbon temperature regime in the firing chamber of the furnace according to [46], characterized by dependency (1):

$$T - T_0 = 1080 \cdot (1 - 0.325 \cdot e^{-0.167 \cdot t} - 0.675 \cdot e^{-2.5 \cdot t}), \tag{1}$$

where  $T$  is the temperature inside the furnace in °C, corresponding to the relevant time  $t$ ;  $T_0$  is the temperature in °C inside the furnace prior to the start of heat impact; and  $t$  is the time in minutes from the start of the test.

Sample nos. 1, 3 and 5 were tested according to the standard temperature regime according to [52], characterized by relationship (2):

$$T - T_0 = 345 \cdot \lg(8 \cdot t + 1), \tag{2}$$

The specimen types, coating thicknesses and resulting flame retardant effectiveness of the structural covers (PE) obtained from the experiments are summarized in Table 2.

Table 2. Types of samples and thickness of the covers for different types of experiments.

| Sample       | Cross-Section    | H, mm | A <sub>ρ</sub> /V, m <sup>-1</sup> | Thickness, mm | Fire Regime | PE, min    |
|--------------|------------------|-------|------------------------------------|---------------|-------------|------------|
| Sample No. 1 | I20B1            | 1700  | 294                                | 15            | S*          | 60         |
| Sample No. 2 | I20B1            | 1700  | 294                                | 15            | H           | 30         |
| Sample No. 3 | I20 B1           | 1700  | 294                                | 50            | S           | 130        |
| Sample No. 4 | I20B1            | 1700  | 294                                | 50            | H           | 93         |
| Sample No. 5 | I40-beam/19.9 tf | 2700  | 134                                | 50            | S           | 243/180 ** |

Note. S\*—standard temperature regime, H—hydrocarbon regime. \*\* Sample no. 5 had a fire resistance limit of 243 min at the deflection critical value [53] and a fire protection efficiency (PE) of 180 min when the critical temperature of 500 °C was reached by the specimen [50].

### 2.2.2. Simulation in SP QuickField 7.0

All structural calculations were performed in SP QuickField 7.0 using the finite element method based on a two-dimensional finite element model [54]. SP QuickField 7.0 (in another version, SP ELCUT) was repeatedly used by the authors to solve thermophysical problems with the purpose of verifying the experimental data [20,55,56].

QuickField packages can be applied to various aspects of thermal model design: heat transfer, temperature distribution, evaluation of local overheating, transient heating processes.

The Heat Transfer module is used to analyse the temperature distribution in static and transient heat transfer processes. The heat sources in the Heat Transfer module can be specified directly and/or imported from other QuickField problems (coupled problems) as Joule Losses. The Heat Transfer module can be used to design and analyse many different electrical and mechanical systems. Steady-state heat transfer analysis is possible not only in 2D Plane-Parallel and 2D axisymmetrical formulations but also as a 3D Extrusion and 3D Import.

Mathematical models of the heat conduction process were applied and the method of solving inverse problems by heat conduction was used according to the system of Equations (3)–(6) [57,58]:

- Equation of heat conduction:

$$C_{\rho}\rho_{\rho}\frac{\partial\theta_{\rho}}{\partial t} = \frac{\partial}{\partial x}(\lambda_{\rho}\frac{\partial\theta_{\rho}}{\partial x}) \quad (3)$$

$$0 < x < d_{\rho}; \theta_{\rho} = \theta_{\rho}(x, t); 0 < t < t_{max}$$

- Initial condition:

$$\theta_{\rho}(x, 0) = \theta_{\rho} \quad (4)$$

- Boundary condition on the surface of the inverse heat conduction task at  $x = d_{\rho}$ :

$$\lambda_{\rho}\frac{\partial\theta_{\rho}(d_{\rho}, t)}{\partial x} = \alpha * [\theta_t - \theta_{\rho}(d_{\rho}, t)], \Gamma_{\text{де}\alpha*} = \alpha_c + \frac{c_0\varepsilon}{\theta_t - \theta_{\rho}(d_{\rho}, t)} \left\{ \left[ \frac{\theta_t + 273.15}{100} \right]^4 - \left[ \frac{\theta_{\rho}(d_{\rho}, t) + 273.15}{100} \right]^4 \right\} \quad (5)$$

- Boundary condition on the inner surface of the fireproof coating at  $x = 0$ :

$$\lambda_{\rho}\frac{\partial\theta_{\rho}(0, t)}{\partial x} = c_{\alpha}\rho_{\alpha} \times \frac{V}{A_{\rho}} \times \frac{\partial\theta_{\rho}(0, t)}{\partial t} \quad (6)$$

where

$x$ —coordinate in the fire protection coating ( $x = 0$  corresponds to the point of contact between the coating and the metal where the sample is measured, temperature  $\theta_a = \theta_{\rho}(0, t)$ );

$c_{\rho}\rho_{\rho}$ —specific heat capacity, J/(kg·K);

$A_{\rho}/V$ —section ratio, mm<sup>-1</sup>;

$\lambda_{\rho}$ —heat conductivity coefficient, W/(m·K);

$t$ —time, s;

$C_0 = 0.57$ ;

$d_{\rho}$ —thickness of fireproof coating, mm;

$t_{max}$ —the maximum heating time of the sample, s;

$\alpha_c$ —heat transfer coefficient on the outer surface of the fireproof coating, W/(m<sup>2</sup>·K);

$\varepsilon = 0.7$ —the degree of blackness of the surface of the mineral coating [59];

$\theta_0$ —initial temperature of the sample, °C;

$\theta_t$ —temperature in the firing furnace, °C.

Initial characteristics of steel: grade C245 [60] density 7800 kg/m<sup>3</sup>; thermal conductivity and heat capacity variable depending on temperature (values taken from the programme reference book). The boundary conditions are presented in Table 3.

**Table 3.** Boundary conditions defined in SP QuickField 7.0.

| Name of the Value  | Value | Information Source |
|--|-------|--------------------|
| Convection heat transfer coefficient with hydrocarbon temperature regime, $W/(m^2K)$ | 50    | [61]               |
| Convection heat transfer coefficient with standard temperature regime, $W/(m^2K)$    | 25    | [61]               |
| Surface absorption coefficient   | 0.5   | [62]               |
| Initial ambient temperature, $^{\circ}C$   | 20    | -                  |
| Density of the thermal insulation cover, $kg/m^3$                                    | 125   | -                  |

For the boundary solutions of the third kind, material density was assumed to be independent of temperature. To solve the problem with boundary conditions of the first kind, then the temperature should be set according to Equations (1) and (2) for the corresponding mode. To determine the characteristics of the fire resistance of structures, mathematical models of the heat conduction process were applied and the method of solving inverse problems of heat conduction was used, defined by the system of Equations (3)–(6).

Based on the obtained experimental temperature–time dependences of the samples, the thermophysical properties of the flexible covers were determined. The finite element diagrams of the modelling samples are shown in Figure 7. The finite element mesh spacing on the faces was set to 20 mm. It was not reasonable to set the grid spacing to less than 20 mm in this task because the calculation time would increase significantly. Further, the grid size was divided automatically under the size of the faces, but there was the possibility to manually adjust the sizes. In each block, the grid was generated automatically.

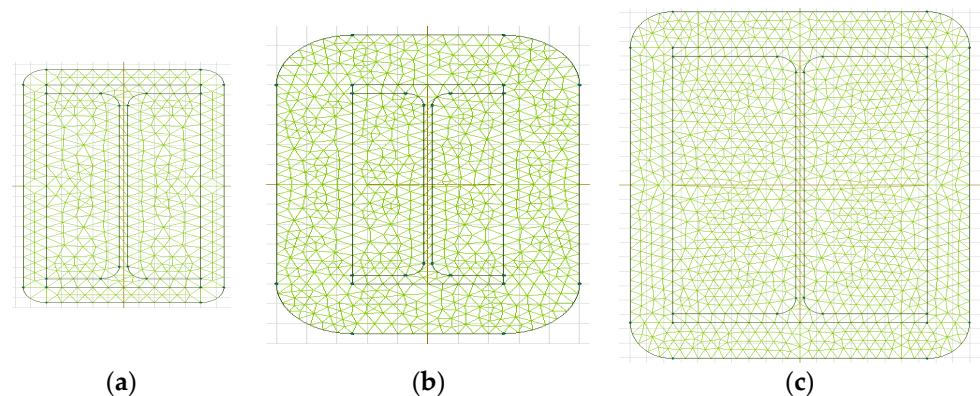


**Figure 7.** Finite element diagrams of the design sections of specimen nos. (a) 1 and 2, (b) 3 and 4, and (c) 5.

### 3. Results

According to the results of the tests, it was established that sample no. 4 with a thickness of 50 mm provided fire protection efficiency under the conditions of exposure to a hydrocarbon combustion regime for 90 min of the steel column of the I-beam section of profile no. 20B1 [51], height 1700 mm, section ratio  $A_p/V = 294 m^{-1}$  [52]. The experiment was terminated in 93 min after the sample reached the critical temperature of  $500^{\circ}C$  in accordance with [50].

During the testing of sample nos. 1–4, no visible changes in the appearance of the samples were recorded (Figure 8).

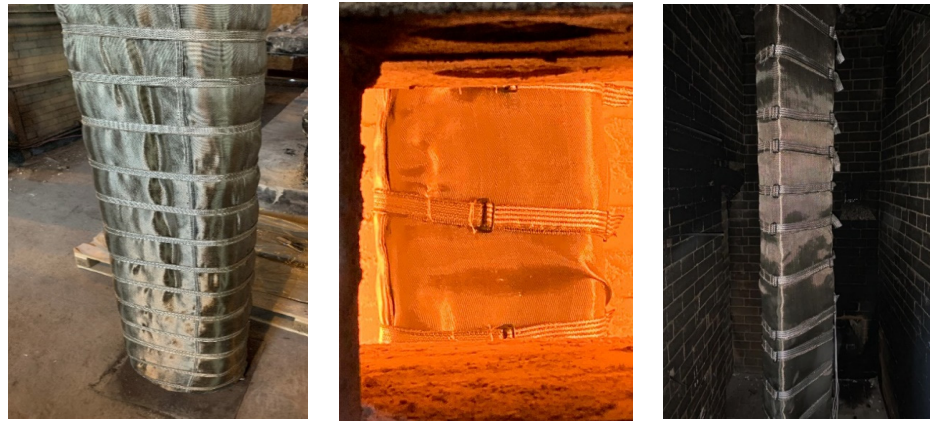


**Figure 8.** Specimen no. 1 before starting the test (**left**), during the test (**centre**) and after the test (**right**).

According to the results of the tests for specimen no. 5, it was found that a cover thickness of 50 mm provided fire protection efficiency under the conditions of exposure to a hydrocarbon mode of combustion of the steel column of the I-beam section of a wide-shelf I-beam with a height of 2700 mm and section ratio  $A_p/V = 134 \text{ m}^{-1}$  [52]. During the test, the outer layer of the shroud was covered with molten basalt, which appeared after prolonged exposure to the standard fire regime (Figure 9).



**Figure 9.** Specimen no. 5 before starting the test (**left**), during the test (**centre**) and after the test (**right**).

Figure 10 shows the graphical dependences of the averaged thermocouple readings under the fire protection cover for the thicknesses of the steel structure. It can be seen that a thickness of 50 mm was optimal for achieving fire protection efficiency of more than 180 min and 243 min in terms of fire resistance loss (critical deflection), in accordance with [53].

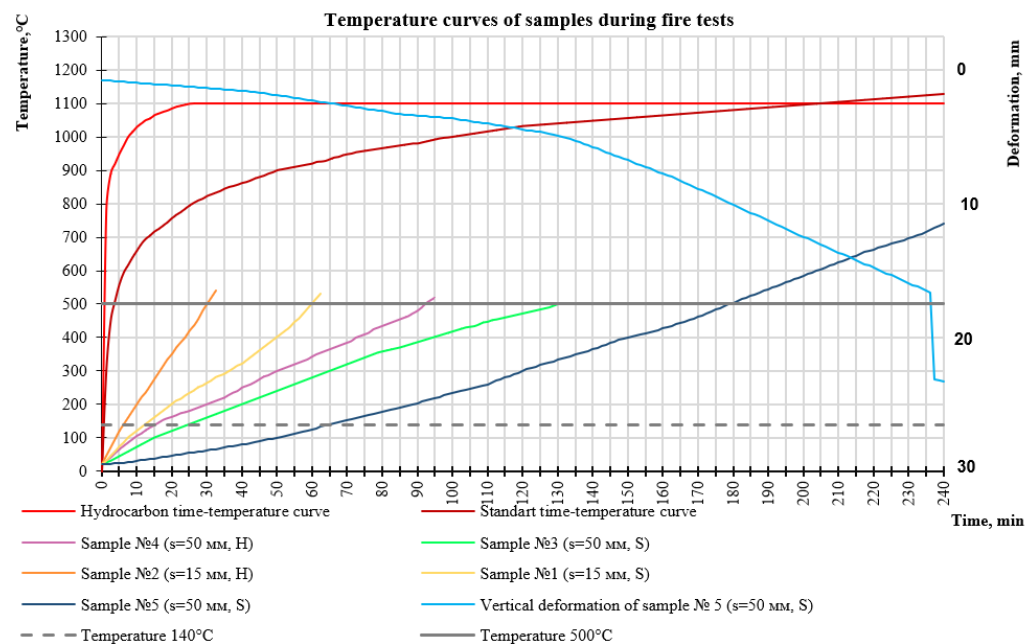


**Figure 10.** Temperature and deformation curves of samples during fire tests.

Also, the dotted line in the graph shows the time to reach 140 °C for the steel I-beam specimen, and it was also possible to estimate the time to reach 140 °C for 15 mm and 50 mm thick composites under different fire regimes.

As can be seen from Figure 10, sample no. 1 with a thickness of 15 mm and density of 130 kg/m<sup>3</sup> reached a temperature of 500 °C in 60 min; sample no. 3 with a thickness of 50 mm reached a temperature of 500 °C in 130 min in standard mode. Sample no. 2 with a thickness of 15 mm and density of 150 kg/m<sup>3</sup> reached 500 °C in 30 min. Sample no. 2 with a thickness of 50 mm reached 500 °C in 93 min in hydrocarbon mode. Heating went uniformly, without kinks, and up to 140 °C was reached on the unheated surface, depending on the thickness of the coating and the fire regime (the greater the thickness, the longer the time to reach the critical temperature). The average temperature according to the readings of the thermometers installed on the metal of sample no. 5 at critical deflection was 749.5 °C, and a temperature of 500 °C was reached after 180 min. After 48 h of testing, the specimen structures were disassembled and the insulating material was removed from the structure. When exposed to temperatures above 500–600 °C, embrittlement and surface failure of the inner layer containing glass fibre occurred.

Figure 11 shows specimen no. 1 after testing and removal of the flame retardant from the I-beam. As can be seen from Figure 11, there was no visible change in the main filler, and the colour, thickness and elasticity of the materials remained unchanged.

Figure 12 shows specimen no. 5 after testing and removal of the flame retardant from the I-beam. As can be seen from Figure 12, there was no visible change in the main filler, and the colour, thickness and elasticity of the materials remained unchanged. The clamping straps were also not damaged.

The inner layer of the glass fabric was completely embrittled and was mostly destroyed when attempting to remove the cover. At the joint of the cover, in places of loose fit, signs of embrittlement and melting were visible. Therefore, the issue of quality joints is one of the most difficult for such fireproof covers.



Figure 11. Specimen no. 1 after testing.



Figure 12. Specimen no. 5 after testing.

In addition, it was of interest to obtain data on the optimum coating thickness under different fire regimes to ensure the same flame retardant performance using simulations.

Figure 13 shows a visualisation of the heating of the specimens in the simulation for 25 min of fire exposure under different fire regimes.

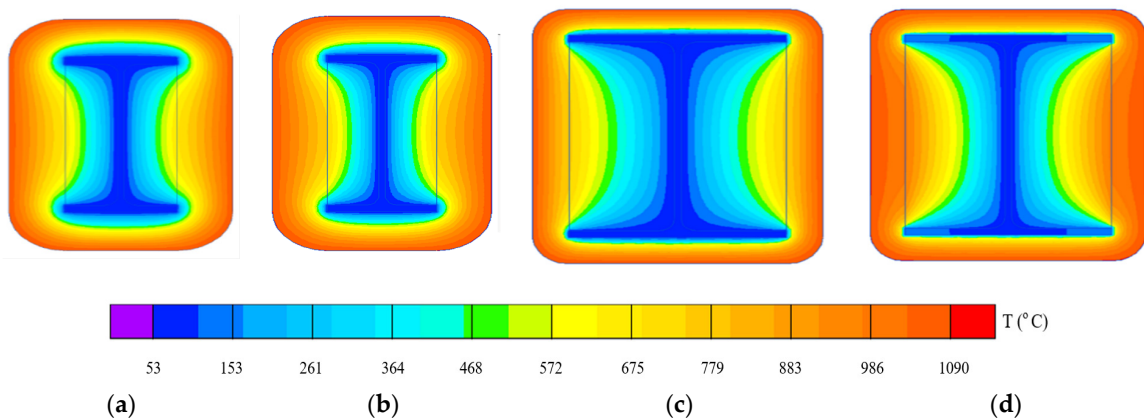
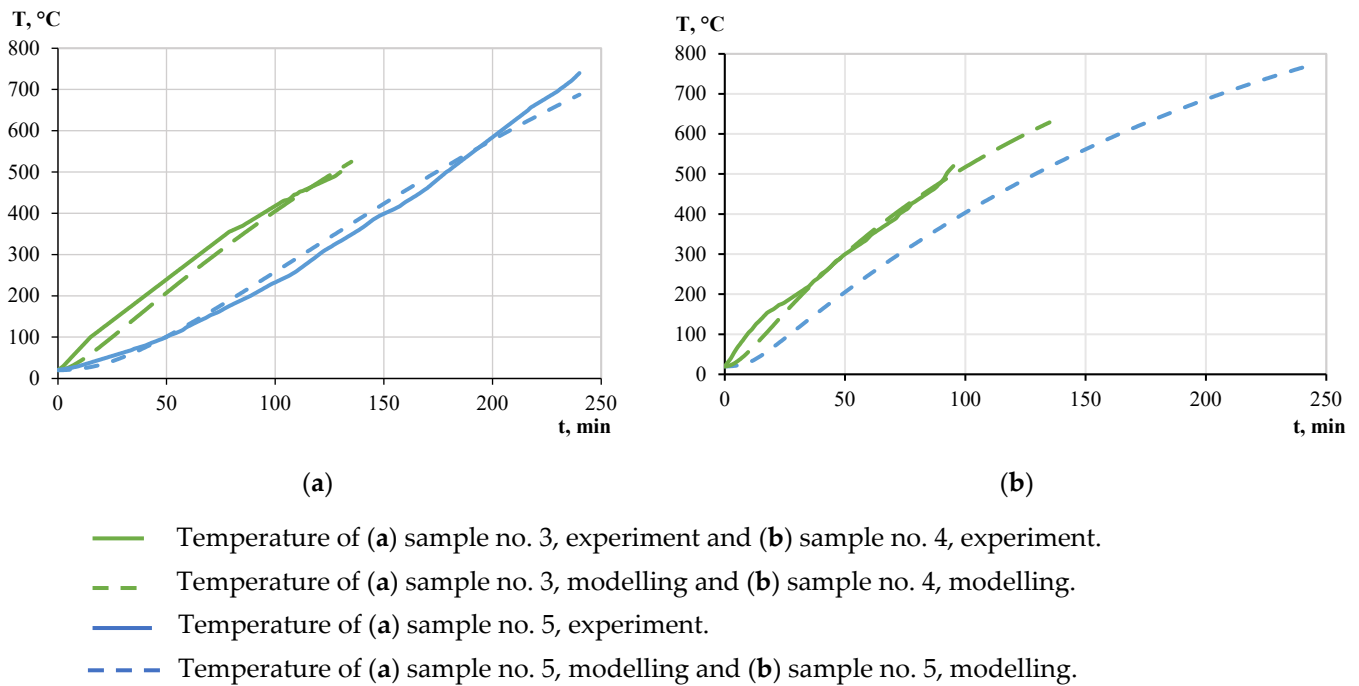


Figure 13. Visualisation of heating of sample nos. 3 and 4 during simulation in S (a) and H (b) modes at 25th min and visualisation of column heating of sample no. 5 during simulation in S (c) and H (d) modes at 25th min.

The temperature variation curves at controlled points on the surface of fire-resistant specimens nos. 3, 4 and 5 during the experiment and simulation are shown in Figure 14.



**Figure 14.** Test and modelling results for (a) no. 3 under S- and (b) nos. 4 and 5 under H- fire regimes (modelling).

The analysis of the modelling results showed that the average difference in the heating temperature of the I-beam structure between the experimental and calculated data under the standard fire regime was not more than 5%. The results of the structural modelling correlated with the results of the fire tests obtained during the experiment.

The calculated fire resistance limit of the structure was 130 min under the standard fire regime for sample no. 3 and 93 min under the hydrocarbon fire regime for sample no. 4. The modelling results correlated with the fire test results obtained from the experiment.

To optimize the consumption of fire protection coatings, calculation models of a column specimen with two types of cross-sections were developed:  $A\rho/V = 294 \text{ m}^{-1}$  and  $A\rho/V = 134 \text{ m}^{-1}$  with different coating thicknesses. The graphs in Figure 15 show the dependence of the time to reach the critical temperature on the coating thickness under the standard and hydrocarbon fire regimes. To obtain a fire protection efficiency of 120 min for a steel column of I-beam cross-section  $294 \text{ m}^{-1}$  in the standard fire regime, it was sufficient to apply a fire protection thickness of 45 mm (Figure 15a); in the hydrocarbon regime at a thickness of 45 mm, the fire protection reached the fire resistance limit R90 (Figure 15b). To obtain the fire resistance limit R120 in the standard fire regime for the sample of steel structure made of the I40 beam ( $134 \text{ m}^{-1}$ ), it was enough to apply fire protection with a thickness of 25 mm instead of 50 mm according to experimental data (Figure 15c); in the hydrocarbon regime, a thickness of 45 mm was required, according to modelling data (Figure 15d).

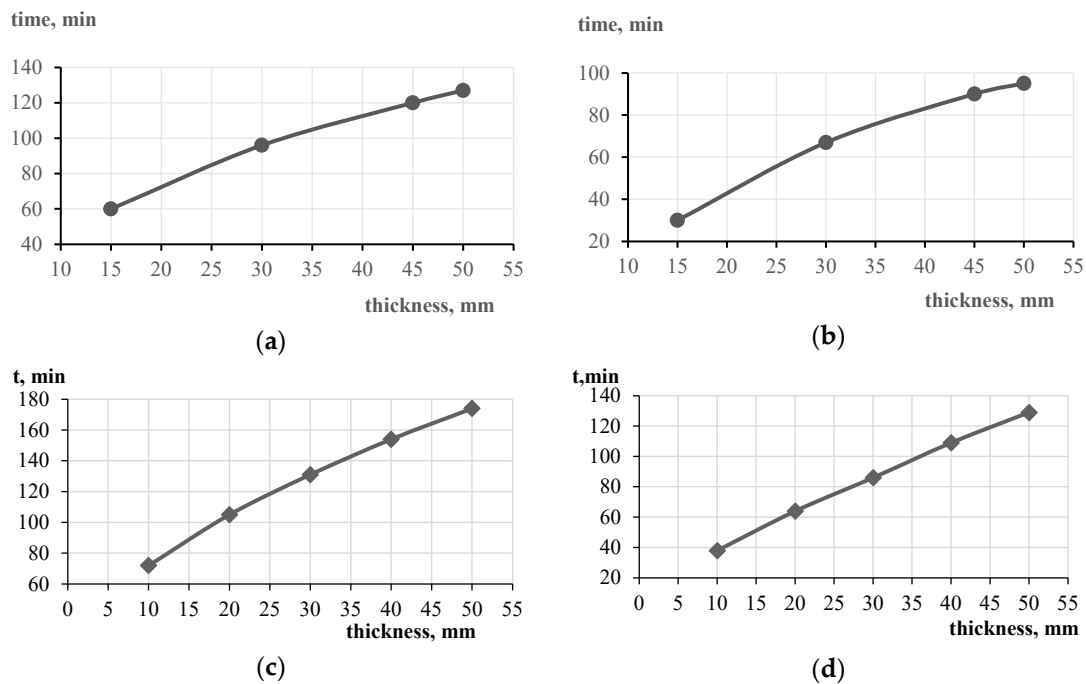


**Figure 15.** Graph of dependence of the time to reach the critical temperature of the specimens with  $A\rho/V 293 \text{ m}^{-1}$  and  $A\rho/V 134 \text{ m}^{-1}$  on the thickness of the protective coating under S- (a,c) and H- (b,d) fire regimes.

When modelling a structure with a fire-protected beam (no. 5), the dependences of the thermophysical characteristics on the temperature were obtained (Table 4).

**Table 4.** Calculated coefficients of thermal conductivity and heat capacity of structural coating for specimen no. 5 obtained from modelling as a function of temperature.

| T, °C                               | 20   | 100  | 200  | 300  | 400  | 500  | 600  | 700  | 800  | 900  | 1000 | 1200 |
|-------------------------------------|------|------|------|------|------|------|------|------|------|------|------|------|
| $\lambda, \text{ W/K}\cdot\text{m}$ | 0.17 | 0.07 | 0.04 | 0.04 | 0.06 | 0.10 | 0.15 | 0.21 | 0.29 | 0.36 | 0.44 | 0.60 |
| $C, \text{ J/kg}\cdot\text{m}$      | 219  | 276  | 348  | 420  | 492  | 564  | 636  | 708  | 780  | 852  | 924  | 1069 |

The coefficients in Table 4 were obtained by fitting the corresponding temperature curves (insulation cover heating) so that the heating matched the experimental data of the average thermocouple readings according to the test reports. These coefficients could then be set again in the heating calculation in SP QuickField 7.0 and checked to see if the model and experimental temperatures matched.

#### 4. Conclusions

The most effective means of fire protection for structures and products are composite materials made of various combinations of non-combustible thermal insulation materials, providing a “dry” method of installation, long service life in harsh conditions, and resistance to hydrocarbon fire regimes. PROMIZOL-MIX PROPLATE coating consists of ultra-thin basalt and ceramic fibres, as well as additional spacers made of various fire-resistant fabrics and aluminium foil.

In this paper, a combined type of coating was presented that, depending on the task, shows good fire protection results due to the combination of the selected layers. It is expedient to use new effective flame retardant materials with the possibility of dry installation in Arctic and Antarctic conditions.

The practical application of this research is that a removable, non-combustible type of fire protection for steel structures providing high fire resistance limits has been obtained.

Such products can be used for steel structures of trestles and decks, structures of offshore platforms, and tunnel structures located in the epicentre of a fire under scenarios calculated in accordance with the concept of fire risk.

In the future, wide application of combined fire protection means is predicted for the development of fire-resistant fabrics for caps, covers and fire curtains using basalt, perlite, aerogel, vermiculite, graphite and other materials. For application in the oil and gas industry, in the construction of tunnels, and at hazardous chemical production facilities, such materials should have resistance to hydrocarbon fire regimes and the spillage of cryogenic liquids, maintainability, and high durability under various climatic conditions.

## 5. Patents

Prusakov, V.A.; Gravit, M.V.; Antonov, S.P. RU2725720C1—Fire-resistant multilayer article for fire protection of building structures. 2020.

**Author Contributions:** Conceptualization, M.G.; methodology, M.G.; software, N.S.; investigation, V.P.; resources, V.P.; data curation, I.K.; writing—original draft preparation, I.K. All authors have read and agreed to the published version of the manuscript.

**Funding:** This research was funded by the Russian Science Foundation (RSF) under grant no. 23-29-00618. URL: <https://rscf.ru/project/23-29-00618/> (accessed on 11 March 2024).

**Institutional Review Board Statement:** Not applicable.

**Informed Consent Statement:** Not applicable.

**Data Availability Statement:** Data are contained within the article.

**Conflicts of Interest:** The authors declare no conflicts of interest.

## References

1. Imran, M.; Liew, M.s.; Nasif, M.S.; Niazi, M.U.K.; Yesreen, A. Hazard Assessment Studies on Hydrocarbon Fire and Blast: An Overview. *J. Comput. Theor. Nanosci.* **2017**, *23*, 1243–1247. [[CrossRef](#)]
2. Kim, J.H.; Baeg, D.Y.; Seo, J.K. Numerical Investigation of Residual Strength of Steel Stiffened Panel Exposed to Hydrocarbon Fire. *J. Ocean Eng. Technol.* **2021**, *35*, 203–215. [[CrossRef](#)]
3. Gravit, M.; Golub, E.; Klementev, B.; Dmitriev, I. Fire protective glass fiber reinforced concrete plates for steel structures under different types of fire exposure. *Buildings* **2021**, *11*, 187. [[CrossRef](#)]
4. Shallcross, D.C. Using concept maps to assess learning of safety case studies—The Piper Alpha disaster. *Educ. Chem. Eng.* **2013**, *8*, e1–e11. [[CrossRef](#)]
5. Zybina, O.; Gravit, M. *Intumescent Coatings for Fire Protection of Building Structures and Materials*; Springer Series on Polymer and Composite Materials; Springer International Publishing: Cham, Switzerland, 2020.
6. Akporjevwe, U.G. The Piper Alpha Disaster—Impacts to Safety. Available online: [https://www.researchgate.net/publication/349278316\\_The\\_Piper\\_Alpha\\_Disaster-Impacts\\_to\\_Safety](https://www.researchgate.net/publication/349278316_The_Piper_Alpha_Disaster-Impacts_to_Safety) (accessed on 24 January 2024).
7. Chen, D.; Werder, E.J.; Stewart, P.A.; Stenzel, M.R.; Gerr, F.E.; Lawrence, K.G.; Groth, C.P.; Huynh, T.B.; Ramachandran, G.; Banerjee, S.; et al. Exposure to volatile hydrocarbons and neurologic function among oil spill workers up to 6 years after the Deepwater Horizon disaster. *Environ. Res.* **2023**, *231*, 116069. [[CrossRef](#)]
8. McClain, C.R.; Nunnally, C.; Benfield, M.C. Persistent and substantial impacts of the Deepwater Horizon oil spill on deep-sea megafauna. *R. Soc. Open Sci.* **2019**, *6*, 191164. [[CrossRef](#)]
9. Evangelista, H.; Sodré, E.D.; Lima, A.C.M.e. Preliminary Investigation on the Atmospheric Dispersion of Pollutants Due to Ferraz Fire. *INCT-APA Annu. Act. Rep.* **2013**, 35–42. [[CrossRef](#)]
10. Pongpiachan, S.; Hattayanone, M.; Pinyakong, O.; Viyakarn, V.; Chavanich, S.A.; Bo, C.; Khumsup, C.; Kittikoon, I.; Hirunyatrakul, P. Quantitative ecological risk assessment of inhabitants exposed to polycyclic aromatic hydrocarbons in terrestrial soils of King George Island, Antarctica. *Polar Sci.* **2017**, *11*, 19–29. [[CrossRef](#)]
11. Gravit, M.; Gumerova, E.; Bardin, A.; Lukinov, V. Increase of Fire Resistance Limits of Building Structures of Oil-and-Gas Complex Under Hydrocarbon Fire. *Adv. Intell. Syst. Comput.* **2018**, *692*, 818–829. [[CrossRef](#)]
12. Eremina, T.; Korolchenko, D. Fire Protection of Building Constructions with the Use of Fire-Retardant Intumescent Compositions. *Building* **2020**, *10*, 185. [[CrossRef](#)]
13. Kandola, B.K.; Luangtriratana, P.; Duquesne, S.; Bourbigot, S. The Effects of Thermophysical Properties and Environmental Conditions on Fire Performance of Intumescent Coatings on Glass Fibre-Reinforced Epoxy Composites. *Materials* **2015**, *8*, 5216–5237. [[CrossRef](#)]

14. Jimenez, M.; Bellayer, S.; Revel, B.; Duquesne, S.; Bourbigot, S. Comprehensive Study of the Influence of Different Aging Scenarios on the Fire Protective Behavior of an Epoxy Based Intumescent Coating. *Ind. Eng. Chem. Res.* **2013**, *52*, 729–743. [[CrossRef](#)]
15. Morys, M.; Häßler, D.; Krüger, S.; Schartel, B.; Hothan, S. Beyond the standard time-temperature curve: Assessment of intumescent coatings under standard and deviant temperature curves. *Fire Saf. J.* **2020**, *112*, 102951. [[CrossRef](#)]
16. Chen, Y.; Jiang, M.; Shan, Y.; Yin, W.; Liu, X.; Hu, L.; Li, P.; Liu, J.; Zhang, C. Plastering Gypsum Construction Method of Steel Structure Wall Face With Anti-Corrosion Coating, and Fireproof Protection Device of Steel Structure Components. CN 110130533 A, 16 August 2019.
17. Elbasuney, S.; Maraden, A. Novel Thermoset Nanocomposite Intumescent Coating Based on Hydroxyapatite Nanoplates for Fireproofing of Steel Structures. *J. Inorg. Organomet. Polym. Mater.* **2020**, *30*, 820–830. [[CrossRef](#)]
18. Mahmud, H.M.I.; Mandal, A.; Nag, S.; Moinuddin, K.A.M. Performance of fire protective coatings on structural steel member exposed to high temperature. *J. Struct. Fire Eng.* **2021**, *12*, 193–211. [[CrossRef](#)]
19. Jiang, S.; Wu, H. An Experimental Investigation on the Fire Resistance of the Integrated Envelope-Fire Protection Material for Steel Buildings. *Prog. Steel Build. Struct.* **2021**, *23*, 77–84. [[CrossRef](#)]
20. Gravit, M.; Shabunina, D.; Shcheglov, N. Thermal Characteristics of Epoxy Fire-Retardant Coatings under Different Fire Regimes. *Fire* **2023**, *6*, 420. [[CrossRef](#)]
21. SP 131.13330.2020 Building Climatology. Available online: <https://docs.cntd.ru/document/573659358> (accessed on 29 January 2024).
22. Kottek, M.; Grieser, J.; Beck, C.; Rudolf, B.; Rubel, F. World Map of the Köppen-Geiger climate classification updated. *Meteorol. Zeitschrift* **2006**, *15*, 259–263. [[CrossRef](#)]
23. Abramov, I.V.; Gravit, M.V.; Gumerova, E.I. Increase in the fire resistance limits of ship and building structures with hydrocarbon fire. *GAS Ind.* **2018**, *768*, 108–117.
24. Palazzi, E.; Fabiano, B. Analytical modelling of hydrocarbon pool fires: Conservative evaluation of flame temperature and thermal power. *Process Saf. Environ. Prot.* **2012**, *90*, 121–128. [[CrossRef](#)]
25. Li, J.; Hao, H. Internal and external pressure prediction of vented gas explosion in large rooms by using analytical and CFD methods. *J. Loss Prev. Process Ind.* **2017**, *49*, 367–381. [[CrossRef](#)]
26. Hassel, M.; Utne, I.B.; Vinnem, J.E. Allision risk analysis of offshore petroleum installations on the Norwegian Continental Shelf—An empirical study of vessel traffic patterns. *WMU J. Marit. Aff.* **2017**, *16*, 175–195. [[CrossRef](#)]
27. Prusakov, V.A.; Gravit, M.V.; Simonenko, Y.B. Superthin Basalt Fiber as the Base of a Matrix of the Fire-Resistant Filling of Deformation Joints in Building Structures. *Glas. Phys. Chem.* **2023**, *49*, 75–80. [[CrossRef](#)]
28. Al-Jadiri, M.S.F.; Said, A.M.I. Reinforced Concrete Columns Insulated by Different Gypsum Layers Exposed to 900 °C One Side Fire Flame. *Eng. Technol. Appl. Sci. Res.* **2023**, *13*, 11586–11592. [[CrossRef](#)]
29. Batiz. Comparative Characteristics of Thermal Insulation Wool Obtained from Various Raw Materials. Available online: <http://batis.ru/kompaniya/eto-interesno/30-sravnitel'naya-kharakteristika-teploizolyatsionnoj-vaty-poluchennyj-iz-razlichnogo-syrya/> (accessed on 24 January 2024).
30. Budykina, T.; Anosova, Y. Thermal resistance of fire retardant materials. *Mag. Civ. Eng.* **2022**, *112*, 11213. [[CrossRef](#)]
31. Pang, Y.; Zhong, Z.; Liu, H.; Rao, L. Research on Fire-Resistant Fabric Properties of Basalt Fiber. *Appl. Mech. Mater.* **2012**, *217–219*, 1151–1154. [[CrossRef](#)]
32. Wang, K.; Fu, C.; Xu, A.; Wu, M.; Jia, L.; Xu, W.; Su, B.; Xia, Z. Skin-friendly and highly fireproof fabric up to 1142 °C weaved by basalt @ polyimide yarns. *Compos. Part B Eng.* **2022**, *246*, 110238. [[CrossRef](#)]
33. Ming, H. Fire-Proof Basalt Fiber Cloth. CN 105088794 A, 25 November 2015.
34. Xiang, W.; Maolin, L.; Xiaolong, T. Multi-Functional Basalt Fiber Fire Blanket. CN 207768955 U, 28 August 2018.
35. Bezas, M.Z.; Nikolaidis, T.N.; Baniotopoulos, C.C. Fire Protection and Sustainability of Structural Steel Buildings with Double-Shell Brickwork Cladding. *Procedia Environ. Sci.* **2017**, *38*, 298–305. [[CrossRef](#)]
36. Mahmood, E.M.; Allawi, A.A.; El-Zohairy, A. Analysis and Residual Behavior of Encased Pultruded GFRP I-Beam under Fire Loading. *Sustainability* **2022**, *14*, 13337. [[CrossRef](#)]
37. Mahmood, E.M.; Ibrahim, T.H.; Allawi, A.A.; El-Zohairy, A. Experimental and Numerical Behavior of Encased Pultruded GFRP Beams under Elevated and Ambient Temperatures. *Fire* **2023**, *6*, 212. [[CrossRef](#)]
38. Sotoodeh, K. Valve operability during a fire. *J. Offshore Mech. Arct. Eng.* **2019**, *141*, 044001. [[CrossRef](#)]
39. Rezayiye, R.K.; Laurent, K.; Nooralishahi, P.; Ibarra-Castaneda, C.; Maldague, X. Thermal Data Augmentation Approach for the Detection of Corrosion in Pipes Using Deep Learning and Finite Element Modelling. *Eng. Proc.* **2023**, *51*, 20. [[CrossRef](#)]
40. Shammazov, I.; Karyakina, E. The LNG Flow Simulation in Stationary Conditions through a Pipeline with Various Types of Insulating Coating. *Nurse Res.* **2023**, *8*, 68. [[CrossRef](#)]
41. Home—Promizol. Available online: <http://tdpromizol.com/home/> (accessed on 2 March 2024).
42. PAO NOVATEK Business: Project Arctic LNG 2 | Arctic LNG 2. Available online: <https://www.novatek.ru/en/business/arctic-lng/> (accessed on 2 March 2024).
43. ASTM E119; Standard Test Methods for Fire Tests of Building Construction and Materials. ASTM International: West Conshohocken, PA, USA, 2022. Available online: <https://www.astm.org/e0119-00a.html> (accessed on 29 January 2024).
44. UL 1709-2017; Standard for Safety Rapid Rise Fire Tests of Protection Materials for Structural Steel. Underwriters Laboratories Inc. (UL): Northbrook, IL, USA, 2017. Available online: <https://docs.cntd.ru/document/550713257> (accessed on 29 January 2024).

45. Vorobev, N.N.; Barinov, D.Y.; Zuev, A.V.; Pakhomkin, S.I. Computational and experimental study of the effective thermal conductivity of fibrous materials. *Proc. VIAM* **2021**, *7*, 95–102. [CrossRef]
46. Sound Insulation, Thermal Insulation and Refractory Materials | MIC-Izol. Available online: <https://mikizol.ru/> (accessed on 24 January 2024).
47. Prusakov, V.A.; Gravit, M.V.; Antonov, S.P. Fire-Resistant Multilayer Article for Fire Protection of Building Structures. RU2725720C1, 3 July 2020.
48. GOST 53295-2009; Russian State Standard, Fire Retardant Compositions for Steel Constructions. General Requirement. Method for Determining Fire Retardant Efficiency. Standartinform Publ.: Moscow, Russia, 2009. Available online: <https://docs.cntd.ru/document/1200071913> (accessed on 29 January 2024).
49. GOST 26020-83; Russian State Standard, Hot-rolled Steel I-Beam with Parallel Flange Edges. Dimensions. IPK Izdatelstvo Standartov: Moscow, Russia, 2003. Available online: <https://internet-law.ru/gosts/gost/21141/> (accessed on 29 January 2024).
50. Eurocode 3: Design of Steel Structures; CEN (European Committee for Standardization): Brussels, Belgium, 2011; pp. 1–78.
51. GOST 30247.1-94; Russian State Standard, Elements of Building Constructions. Fire-Resistance Test Methods. Loadbearing and Separating Constructions. IPK Izdatelstvo Standartov: Moscow, Russia, 1995. Available online: <https://docs.cntd.ru/document/9055247> (accessed on 24 January 2024).
52. GOST 30247.0-94; Russian State Standard, Elements of Building Constructions. Fire-resistance Test Methods. General Requirements. IPK Izdatelstvo Standartov: Moscow, Russia, 2003. Available online: <https://docs.cntd.ru/document/9055248> (accessed on 29 January 2024).
53. EN 1363-2:1999; Fire Resistance Tests—Part 2: Alternative and Additional Procedures. CEN (European Committee for Standardization): Brussels, Belgium, 2001.
54. QuickField Support Site. Available online: <https://quickfield.com/> (accessed on 29 January 2024).
55. Gravit, M.; Shabunina, D.; Nedryshkin, O. The Fire Resistance of Transformable Barriers: Influence of the Large-Scale Factor. *Fire* **2023**, *6*, 294. [CrossRef]
56. Gravit, M.; Shabunina, D. Numerical and Experimental Analysis of Fire Resistance for Steel Structures of Ships and Offshore Platforms. *Fire* **2022**, *5*, 9. [CrossRef]
57. Wang, J.X.; Liu, K.; Zhao, C.S.; Wang, Z.L. Research on the theoretical calculation method of dynamic response of the stiffened plate on the accommodation of offshore platforms under blast. *Chuan Bo Li Xue/J. Sh. Mech.* **2020**, *24*, 1495–1506. [CrossRef]
58. Kim, T.K.; Kim, S.K.; Lee, J.M. Dynamic Response of Drill Floor Considering Propagation of Blast Pressure Subsequent to Blowout. *Appl. Sci.* **2020**, *10*, 8841. [CrossRef]
59. Kung, F.; Yang, M.C. Improvement of the Heat-Dissipating Performance of Powder Coating with Graphene. *Polymer* **2020**, *12*, 1321. [CrossRef]
60. GOST 27772-2015; Russian State Standard, Rolled Products for Structural Steel Constructions. General Specifications. Standartinform Publ.: Moscow, Russia, 2016. Available online: <https://docs.cntd.ru/document/1200133727> (accessed on 29 January 2024).
61. EN 1991-1-2; Eurocode 1: Actions on Structures—Part 1-2: General Actions—Actions on Structures Exposed to Fire. CEN (European Committee for Standardization): Brussels, Belgium, 2002.
62. Markus, E.S.; Snegirev, A.Y.; Kuznetsov, E.A. *Numerical Simulation of a Fire Using Fire Dynamics*; St. Petersburg Polytech-Press: St. Petersburg, Russia, 2021.

**Disclaimer/Publisher’s Note:** The statements, opinions and data contained in all publications are solely those of the individual author(s) and contributor(s) and not of MDPI and/or the editor(s). MDPI and/or the editor(s) disclaim responsibility for any injury to people or property resulting from any ideas, methods, instructions or products referred to in the content.